

Topological superconducting phase in a non-Hermitian Kitaev chain with staggered pairing imbalance

Xiao-Jue Zhang¹, Rong Lü^{2,3}, and Qi-Bo Zeng^{1*}

¹*Department of Physics, Capital Normal University, Beijing 100048, China*

²*State Key Laboratory of Low-Dimensional Quantum Physics,*

Department of Physics, Tsinghua University, Beijing 100084, China and

³*Collaborative Innovation Center of Quantum Matter, Beijing 100084, China*

We introduce a one-dimensional non-Hermitian Kitaev chain with staggered imbalance in the p -wave superconducting pairing. By tuning the chemical potential and the pairing imbalance, we find that the eigenenergy spectrum undergoes real-to-complex transitions, and the spectral gap can change from a real to an imaginary line gap. The pairing imbalance significantly enlarges the parameter region supporting a topological superconducting phase. Remarkably, we show that a topologically nontrivial phase hosting Majorana zero modes can be induced by varying the pairing imbalance, even in the regime of strong chemical potential. The gap-closing points and phase boundaries are determined analytically, and the resulting phase diagrams are characterized by a nonzero topological invariant. Furthermore, we identify the existence of Majorana zero modes and finite-energy Majorana edge modes in this system. Our results reveal exotic phenomena arising from imbalanced pairing and establish a new platform for exploring topological superconductivity in non-Hermitian systems.

I. INTRODUCTION

Topological superconductors (TSCs) have been extensively investigated over the past two decades as promising platforms for realizing Majorana fermions [1–6]. In their topologically nontrivial phases, TSCs host Majorana zero modes (MZMs) localized at system boundaries, which obey non-Abelian statistics and are therefore of central interest for fault-tolerant quantum computation based on braiding operations [7–11]. A wide variety of theoretical proposals have been put forward to realize MZMs, including two-dimensional p -wave superconductors [12–14], superconductor heterostructures coupled to topological insulators [15] or semiconductors [16–19], as well as other solid-state platforms [20, 21]. In addition, TSC phases have been explored in superfluid He-3 [22–24], ultracold atomic gases [25–31], and chains of magnetic atoms on superconducting substrates [32–34]. Among these platforms, one-dimensional semiconductor-superconductor heterostructures have attracted particular attention [17–19], and signatures of MZMs in such systems have been actively investigated both theoretically [35–40] and experimentally [41–48].

A paradigmatic lattice model for one-dimensional topological superconductivity is the Kitaev chain proposed in Ref. [49]. Since then, numerous extensions of the Kitaev model have been explored. These include studies of periodic, quasiperiodic, and disordered potentials and their effects on MZMs [50–55], as well as Kitaev chains with long-range hopping and/or pairing [56–61]. In addition, generalized Kitaev models with modulated p -wave pairing and hopping have been studied in both one and two dimensions [62–65]. Furthermore,

inhomogeneous or periodically varying superconductivity has been shown to substantially modify the topological properties of Kitaev chains [66–69]. In parallel, non-Hermitian systems have attracted considerable attention as effective descriptions of open quantum systems in recent years [70–73]. The presence of non-Hermiticity can give rise to phenomena that are absent in Hermitian settings, such as exceptional points [74] and the non-Hermitian skin effect [75, 76], which profoundly alters the nature of topological phases, including possible breakdowns of bulk-boundary correspondence [77]. Motivated by these developments, Kitaev chains have been extended to non-Hermitian regimes, where the effects of gain and loss on topological superconductivity and MZMs have been investigated [78–86]. In particular, several non-Hermitian Kitaev chain models with imbalanced pair creation and annihilation were shown to exhibit exotic topological properties [80, 82–84]. It will be interesting to ask if the pairing imbalance becomes spatially modulated, how the topological superconducting phase and MZMs will behave in such non-Hermitian systems.

In this work, we study a one-dimensional non-Hermitian Kitaev chain with staggered imbalance in the superconducting pairing, which effectively describes gain and loss processes associated with pair creation and annihilation. By tuning the chemical potential and the pairing imbalance, we find that the eigenenergy spectrum undergoes real-to-complex transitions, and the spectral gap can change from a real to an imaginary line gap. The corresponding transition points and gap-closing conditions are determined analytically from the momentum-space spectrum. We further show that the presence of pairing imbalance substantially enlarges the parameter region supporting a topologically nontrivial superconducting phase compared with the Hermitian limit. Remarkably, due to the interplay between the chemical potential and the staggered pairing imbalance, the topologi-

* zengqibo@cnu.edu.cn

cal phase and Majorana zero modes can persist even in the regime of arbitrarily large chemical potential, provided that the imbalances are introduced in an alternating manner. The nontrivial phases are characterized by a nonzero topological invariant, and the resulting phase diagrams are presented. In addition, we identify a regime in which Majorana zero modes coexist with finite-energy Majorana edge modes. Our results demonstrate that non-Hermitian pairing imbalance can play a constructive role in stabilizing topological superconductivity and provide a versatile platform for exploring topological phases in non-Hermitian superconducting systems.

The remainder of this paper is organized as follows. In Sec. II, we introduce the model Hamiltonian of the one-dimensional Kitaev chain with staggered pairing imbalance. In Sec. III, we analyze the eigenenergy spectrum and the associated line gaps. The topological phases and Majorana edge modes are investigated in Sec. IV. Finally, Sec. V summarizes our results.

II. MODEL HAMILTONIAN

We consider a one-dimensional lattice model with staggered imbalance in the p -wave superconducting pairing. A schematic illustration of the lattice under open boundary conditions (OBCs) is shown in Fig. 1. Owing to the staggered pairing imbalance, each unit cell contains two sublattice sites, labeled A and B. The system is described by the Hamiltonian

$$\begin{aligned} H = & - \sum_{j=1}^N \mu \left(c_{j,A}^\dagger c_{j,A} + c_{j,B}^\dagger c_{j,B} \right) \\ & - \sum_{j=1}^N t \left(c_{j,B}^\dagger c_{j,A} + h.c. \right) - \sum_{j=1}^{N-1} t \left(c_{j+1,A}^\dagger c_{j,B} + h.c. \right) \\ & + \sum_{j=1}^N \left[(\Delta + \gamma_1) c_{j,B}^\dagger c_{j,A}^\dagger + (\Delta - \gamma_1) c_{j,A} c_{j,B} \right] \\ & + \sum_{j=1}^{N-1} \left[(\Delta + \gamma_2) c_{j+1,A}^\dagger c_{j,B}^\dagger + (\Delta - \gamma_2) c_{j,B} c_{j+1,A} \right]. \end{aligned} \quad (1)$$

Here, $c_{j,\alpha}$ ($c_{j,A}^\dagger$) annihilates (creates) a spinless fermion at sublattice site $\alpha = A, B$ in the j th unit cell. The total number of unit cells is N , corresponding to a chain length $L = 2N$. The chemical potential μ is taken to be uniform throughout the lattice. The parameter t denotes the nearest-neighbor hopping amplitude, and throughout this work we set $t = 1$ as the energy unit. The quantity Δ represents the amplitude of the p -wave superconducting pairing, while γ_1 and γ_2 characterize the imbalance of the pairing strength on the intra- and intercell bonds, respectively. Physically, these imbalances originate from gain and loss processes associated with pair creation and annihilation. As a result, the Hamiltonian in Eq. (1) is intrinsically non-Hermitian and exhibits properties ab-

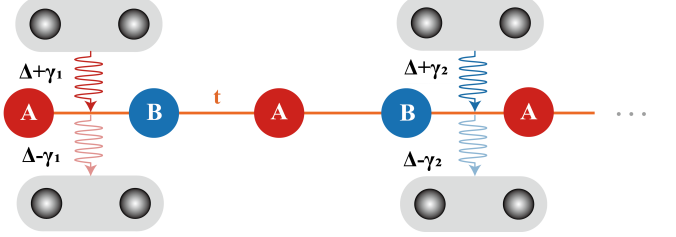


FIG. 1. (Color online) Schematic illustration of the one-dimensional Kitaev chain with staggered p -wave superconducting pairing imbalance under open boundary conditions. Each unit cell contains two sites, labeled A and B, with a uniform chemical potential μ . The orange lines denote nearest-neighbor hopping with amplitude t . The gray shaded regions indicate staggered superconducting pairing terms $\Delta \pm \gamma_{1,2}$ on the intra- and intercell bonds, respectively, which give rise to non-Hermiticity through imbalanced pair creation and annihilation.

sent in its Hermitian counterpart.

A. Real-space Bogoliubov–de Gennes formulation

The eigenenergy spectrum of the Hamiltonian in Eq. (1) under OBC is obtained via exact diagonalization within the Bogoliubov–de Gennes (BdG) formalism. We introduce quasiparticle operators

$$\eta_{n,\alpha} = \sum_{j=1}^N \left[u_{n,j\alpha} c_{n,j\alpha}^\dagger + v_{n,j\alpha} c_{n,j\alpha} \right], \alpha \in \{A, B\} \quad (2)$$

where n labels the eigenstates of the system. The corresponding eigenstates $|\Psi_n\rangle$ satisfy the Schrödinger equation $H|\Psi_n\rangle = E_n|\Psi_n\rangle$. Each eigenstate can be represented as a $2L$ -component Nambu spinor $|\Psi_n\rangle = [u_{n,1A}, u_{n,1B}, \dots, v_{n,jA}, v_{n,jB}, \dots]^T$, and the Hamiltonian is cast into a $2L \times 2L$ BdG matrix, whose eigenvalues yield the full spectrum.

To characterize the localization properties of the eigenstates, we employ the inverse participation ratio (IPR), defined as

$$\text{IPR}_n = \sum_{j,\alpha} (|u_{n,j\alpha}|^4 + |v_{n,j\alpha}|^4). \quad (3)$$

For extended states, the IPR scales to zero in the thermodynamic limit, whereas it remains finite for localized states.

B. Momentum-space Hamiltonian

Under periodic boundary conditions (PBCs), the Hamiltonian can be Fourier transformed into momentum space. Introducing the Nambu spinor $C_k^\dagger =$

$\begin{bmatrix} c_{k,A}^\dagger & c_{k,B}^\dagger & c_{-k,A} & c_{-k,B} \end{bmatrix}$, the Hamiltonian takes the form

$$H = \frac{1}{2} \sum_k C_k^\dagger h(k) C_k, \quad (4)$$

$$h(k) = \begin{bmatrix} -\mu & -t(1+e^{-ik}) & 0 & -(\Delta+\gamma_1) + (\Delta+\gamma_2)e^{-ik} \\ -t(1+e^{ik}) & -\mu & (\Delta+\gamma_1) - (\Delta+\gamma_2)e^{ik} & 0 \\ 0 & (\Delta-\gamma_1) - (\Delta-\gamma_2)e^{-ik} & 0 & t(1+e^{ik}) \\ -(\Delta-\gamma_1) + (\Delta-\gamma_2)e^{ik} & 0 & t(1+e^{ik}) & \mu \end{bmatrix}. \quad (5)$$

Diagonalizing $h(k)$ yields the energy dispersion relation (omitting the overall factor $1/2$),

$$E^2(k) = \mu^2 - \gamma_1^2 - \gamma_2^2 + 2\gamma_1\gamma_2 \cos k + 2t^2(1 + \cos k) + 2\Delta^2(1 - \cos k) \pm 2\sqrt{2t^2\mu^2(1 + \cos k) - [t^2(1 + \cos k)^2 + \Delta^2(1 - \cos^2 k)](\gamma_1 - \gamma_2)^2}. \quad (6)$$

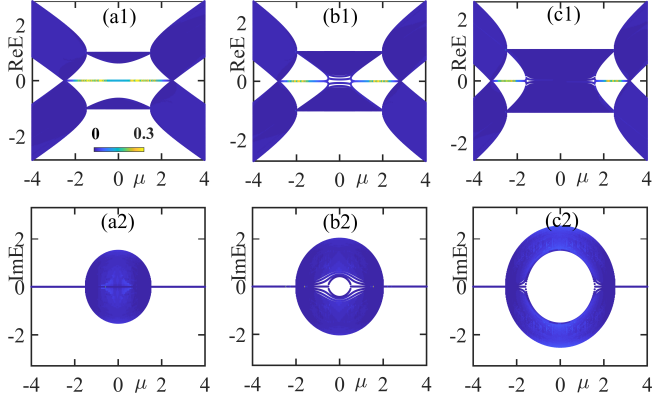


FIG. 2. (Color online) Real and imaginary parts of the eigenenergy spectrum as a function of chemical potential μ for different values of γ_1 with $\gamma_2 = 0$. Panels (a)–(c) correspond to (a) $\gamma_1 = 1.5$, (b) $\gamma_1 = 2.0$, (c) $\gamma_1 = 2.5$. The color scale denotes the inverse participation ratio (IPR) of the eigenstates. Other parameters are $t = 1$, $\Delta = 1$, and system size $L = 2N = 200$.

From Eq. (6), the gap-closing conditions and the phase boundaries between topologically trivial and nontrivial phases can be determined analytically. In the following sections, we analyze the spectral properties of the model and investigate the resulting non-Hermitian topological superconducting phases and Majorana edge modes.

III. EIGENERGY SPECTRUM AND ENERGY GAPS

We first analyze the eigenenergy spectrum for the case $\gamma_2 = 0$, corresponding to pairing imbalance introduced on alternating bonds. Figures 2(a1) and 2(a2) display the real and imaginary parts of the spectrum as functions of the chemical potential μ , where the color scale denotes

where the BdG Hamiltonian $h(k)$ is given by

Diagonalizing $h(k)$ yields the energy dispersion relation (omitting the overall factor $1/2$),

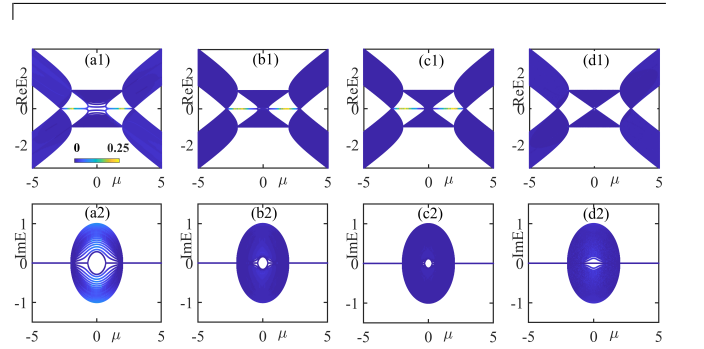


FIG. 3. (Color online) Eigenenergy spectrum for the system with $\gamma_1 = 2.0$ and $\gamma_2 = 0$ for different system size: (a) $L = 100$, (b) $L = 400$, and (c) $L = 800$ under open boundary conditions. Panel (d) shows the corresponding spectrum under periodic boundary conditions. Other parameters are $t = 1$, $\Delta = 1$.

the IPR of the eigenstates. For $|\gamma_1| < 2t$, the real part of the spectrum exhibits a finite gap, while the imaginary part remains gapless, indicating the presence of a real line gap. The real gap closes at

$$\mu = \pm \sqrt{4t^2 + (\gamma_1 - \gamma_2)^2}, \quad (7)$$

which follows from Eq. (6) by setting $k = 0$.

At $\gamma_1 = 2t$, the real line gap further closes at $\mu = 0$, and an imaginary line gap opens, as shown in Fig. 2(b). In finite systems under open boundary conditions, the real part of the spectrum appears gapless in a small region around $\mu = 0$ [Fig. 2(b1)], which is a finite-size effect. In particular, near the gap-closing point, the OBC spectrum can deviate noticeably from the PBC spectrum. By increasing the system size, the OBC spectrum converges to the PBC result. In Fig. 3, we present the eigenenergy spectra for different system sizes at $\gamma_1 = 2t$ and $\gamma_2 = 0$. As the system size increases from $L = 100$ to $L = 800$, the apparent gapless region in the real part of the spectrum around $\mu = 0$ progressively shrinks, while

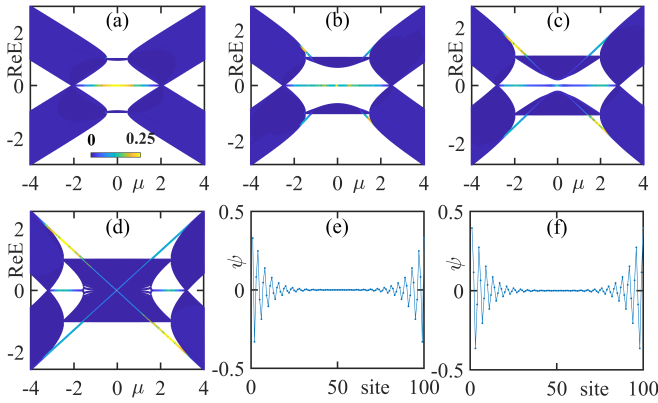


FIG. 4. (Color online) Real and imaginary parts of the eigenenergy spectrum as a function of chemical potential μ for different values of γ_2 with $\gamma_1 = 0$. Panels (a)–(d) correspond to (a) $\gamma_2 = 0.5$, (b) $\gamma_2 = 1.5$, (c) $\gamma_2 = 2.0$, (d) $\gamma_2 = 2.5$. Panels (e) and (f) show the spatial probability distributions of the Majorana zero modes and finite-energy Majorana edge modes, respectively. Other parameters are $t = 1$, $\Delta = 1$, and system size $L = 2N = 200$.

the gap in the imaginary part near $\mu = 0$ also decreases. This size dependence indicates that $\gamma_1 = 2t$ and $\gamma_2 = 0$ corresponds to a critical point at which the real line gap closes and an imaginary line gap begins to open at $\mu = 0$. This behavior is consistent with the spectrum obtained under periodic boundary conditions, shown for comparison in Fig. 3(d).

As the pairing imbalance γ_1 is further increased, the gapless region in the real part of the spectrum expands, accompanied by a widening of the imaginary line gap, as shown in Fig. 2(c). The imaginary line gap closes at

$$\mu = \pm \sqrt{-4\Delta^2 + (\gamma_1 + \gamma_2)^2}, \quad (8)$$

which can be obtained from Eq. (6) by setting $k = \pi$ and requiring the imaginary part of the spectrum to vanish. For larger values of the chemical potential, $|\mu| > \sqrt{-4\Delta^2 + (\gamma_1 + \gamma_2)^2}$, the spectrum becomes gapped again in the real part. Similar spectral features are observed for nonzero γ_2 , indicating that these real–imaginary gap transitions are generic in the presence of staggered pairing imbalance.

In addition, the inspection of the imaginary parts of the spectrum in Fig. 2 shows that, for sufficiently large $|\mu|$, the eigenenergies become purely real, signaling a complex-to-real transition in the spectrum. For the representative case $t = \Delta = 1$, the transition occurs at $\mu = \pm|\gamma_1 - \gamma_2|$. Overall, the introduction of pairing imbalance in the non-Hermitian Kitaev chain leads to rich spectral behavior, including real–complex transitions and the conversion between real and imaginary line gaps. These features play a crucial role in determining the topological phases of the system, as discussed in the following section.

IV. TOPOLOGICAL SUPERCONDUCTING PHASE

We now investigate the topological properties of the non-Hermitian Kitaev chain with staggered pairing imbalance. For the present model, no non-Hermitian skin effect is observed, and the bulk–boundary correspondence remains valid. As a result, the phase boundaries of the topological superconducting phases can be determined from the gap-closing conditions of the bulk spectrum under periodic boundary conditions.

As shown in Fig. 2, Majorana zero modes appear inside the spectral gap in the topologically nontrivial regime. For $|\gamma_1| < 2t$, the nontrivial phase occurs when

$$|\mu| < \sqrt{4t^2 + (\gamma_1 - \gamma_2)^2}. \quad (9)$$

Compared with the Hermitian Kitaev chain, where MZMs exist only for $|\mu| < 2t$, the presence of pairing imbalance substantially enlarges the parameter region supporting a topological superconducting phase.

When $|\gamma_1| > 2t$ and $|\Delta| < 2t$, the topologically nontrivial phase is realized within the window

$$\sqrt{-4\Delta^2 + (\gamma_1 + \gamma_2)^2} < |\mu| < \sqrt{4t^2 + (\gamma_1 - \gamma_2)^2}, \quad (10)$$

which follows from the gap-closing conditions at $k = 0$ and $k = \pi$ in Eq. (6). Notably, if either γ_1 or γ_2 vanishes, or γ_1 and γ_2 are of opposite signs, a finite interval of μ satisfying Eq. (10) always exists. This implies that a topologically nontrivial phase with MZMs can persist even for arbitrarily large chemical potential, in sharp contrast to the Hermitian Kitaev chain. In the following, we will investigate the properties of the edge modes and calculate the topological invariant characterizing the nontrivial phase.

A. Coexistence of zero- and finite-energy Majorana edge modes

For the case with $\gamma_1 = 0$ and $\gamma_2 \neq 0$, the parameter regions supporting MZMs are qualitatively similar, as shown in Fig. 4. The spatial profiles of the MZMs are presented in Fig. 4(e). In addition to the zero-energy modes, finite-energy Majorana edge modes emerge when γ_2 becomes sufficiently large, as illustrated in Fig. 4(b). With increasing γ_2 , these finite-energy edge modes extend over a broader parameter region and may even enter the bulk spectrum, as shown in Figs. 4(c) and 4(d). In total, there are four finite-energy edge modes, with their spatial distributions shown in Fig. 4(f). The corresponding eigenenergies depend approximately linearly on the chemical potential μ . Again, note that in Fig. 4(c), the gap should be closed at $\mu = 0$, but for finite size system, the gap seems still open in this case. By increasing the system size, the gap will become closed.

When both γ_1 and γ_2 are nonzero, similar spectral and topological features are observed, as shown in Figs. 5(a)

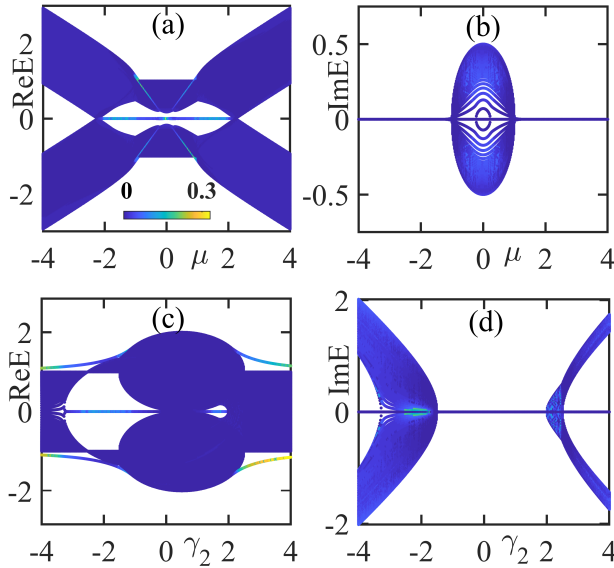


FIG. 5. (Color online) Eigenenergy spectrum of the non-Hermitian Kitaev chain for finite pairing imbalance in both intra- and intercell pairing terms. Panels (a) and (b) show the real and imaginary parts of the spectrum, respectively, as functions of the chemical potential μ for $\gamma_1 = 0.5$ and $\gamma_2 = 1.5$. Panels (c) and (d) show the real and imaginary parts of the spectrum, respectively, as functions of the inter-cell pairing imbalance γ_2 for $\gamma_1 = 0.5$ and $\mu = 2$. The system size is $L = 200$.

and 5(b). The real part of the spectrum becomes gapless at $\mu = 0$ when $|\gamma_1 + \gamma_2| = 2t$, and MZMs appear for $|\mu| < \sqrt{4t^2 + (\gamma_1 - \gamma_2)^2}$, consistent with Eq. (10). For $|\mu| > |\gamma_1 - \gamma_2|$, the spectrum becomes purely real, signaling a complex-to-real transition. Finite-energy edge modes can again be observed inside the bulk spectrum [Fig. 5(a)].

Figures 5(c) and 5(d) show the spectrum as a function of γ_2 for $\gamma_1 = 0.5$ and $\mu = 2t$. In this case, the two topologically nontrivial regions are asymmetric with respect to γ_2 , owing to the simultaneous presence of intra- and intercell pairing imbalance. As γ_1 increases, the nontrivial region at positive γ_2 gradually shrinks and eventually disappears, whereas the region at negative γ_2 remains robust. Finite-energy edge modes emerge when $|\gamma_2|$ becomes sufficiently large, and the spectrum undergoes a real-complex transition, as shown in Fig. 5(d).

To gain further insight into the emergence of finite-energy Majorana edge modes, we rewrite the Hamiltonian in terms of Majorana operators by introducing $c_{j,A} = \frac{1}{2}(f_{2j-1,1} + if_{2j-1,2})$ and $c_{j,B} = \frac{1}{2}(f_{2j,1} + if_{2j,2})$, where the Majorana operators satisfy $\{f_{m,a}, f_{n,b}\} = 2\delta_{m,n}\delta_{a,b}$ with $a, b \in \{1, 2\}$. The Dirac fermion is now expressed as the combination of two Majorana fermions, denoted by $f_{2j-1,1}$ and $f_{2j-1,2}$ for the A site, and $f_{2j,1}$ and $f_{2j,2}$ for the B site in the j th unit cell, respectively. In this representation, the Kitaev chain maps onto a ladder model composed of Majorana fermions, as schematically illustrated in Fig. 6. The chemical potential μ induces

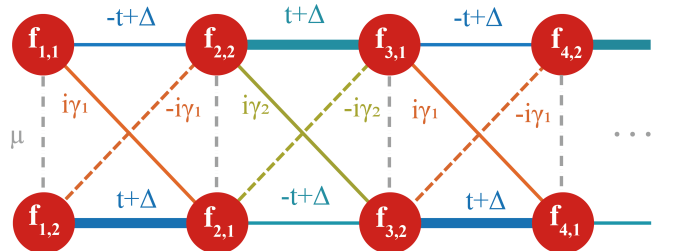


FIG. 6. (Color online) Schematic illustration of the effective two-leg ladder representation of the one-dimensional Kitaev chain in the Majorana fermion basis. Red solid circles denote Majorana fermion operators, and the connecting lines indicate the couplings induced by chemical potential, hopping and imbalanced superconducting pairing terms.

inter-leg couplings, while the hopping t and SC pairing term Δ generate nearest-neighbor couplings along each leg. The staggered pairing imbalance further introduces diagonal couplings between Majorana fermions on opposite legs.

The interplay among these couplings leads to distinct patterns of Majorana dimerization, which in turn give rise to both zero- and finite-energy edge states. The ladder structure can be viewed as comprising four coupled Su-Schrieffer-Heeger (SSH)-type chains: the upper leg, the lower leg, and two zigzag chains formed by the $f_{j,1}$ and $f_{j,2}$ Majorana operators, respectively. In the absence of diagonal couplings, corresponding to vanishing or small pairing imbalance, one of the two legs can realize a nontrivial SSH phase for small μ , depending on the sign of Δ . For example, when $\Delta > 0$, the upper leg is topologically nontrivial while the lower leg remains trivial, leaving the Majorana fermions $f_{1,1}$ and $f_{N,2}$ unpaired at the two ends of the system and giving rise to Majorana zero modes. As the pairing imbalance increases, particularly when $|\gamma_2| > |\gamma_1|$, both zigzag SSH chains become topologically nontrivial. In this regime, the Majorana modes $f_{1,1}$ and $f_{1,2}$ remain unpaired at the left end, while $f_{N,1}$ and $f_{N,2}$ remain unpaired at the right end. The finite inter-leg coupling μ hybridizes these edge Majorana modes locally, lifting their energies away from zero and generating finite-energy Majorana edge states. Therefore, this Majorana ladder picture provides an intuitive and unified explanation for the coexistence of Majorana zero modes and finite-energy edge modes observed in our system.

The finite-energy edge modes are not topologically protected in the same sense as the Majorana zero modes, and their eigenenergies vary continuously with the chemical potential and the pairing imbalance, as shown in Figs. 5(a) and 5(c). In particular, the approximately linear dependence of these edge-mode energies on μ can be understood using the approach developed in Ref. [69]. Notably, in the present non-Hermitian system, Majorana zero modes and finite-energy edge modes can coexist within the same parameter regime. This behavior con-

trasts with the Hermitian Kitaev chain with staggered superconducting pairing studied in Ref. [69], where zero-energy and finite-energy edge modes appear in distinct regions of parameter space.

B. Topological invariant and phase diagram

The topological superconducting phase is characterized by a \mathbb{Z}_2 topological invariant defined in terms of the Pfaffian [49]. Although the pairing imbalance renders the Hamiltonian non-Hermitian, the system does not exhibit the non-Hermitian skin effect, and the bulk spectrum under periodic and open boundary conditions remains consistent when the system size is large enough. As a result, the topology can be characterized using a line-gap classification. When a real or imaginary line gap is present, the system admits a well-defined \mathbb{Z}_2 topological invariant.

$$A(k) = i \begin{bmatrix} 0 & -(\Delta + \gamma_1) + (\Delta + \gamma_2)e^{-ik} & -t(1 + e^{-ik}) \\ (\Delta + \gamma_1) - (\Delta + \gamma_2)e^{ik} & 0 & -t(1 + e^{ik}) \\ \mu & t(1 + e^{-ik}) & \mu \end{bmatrix} \quad (11)$$

which is manifestly skew-symmetric at $k = 0, \pi$. The Pfaffian $Pf[A(k)]$ is in general complex due to non-Hermiticity. However, as long as the system possesses a real or imaginary line gap, the Pfaffian phase can be chosen continuously across the Brillouin zone, allowing the definition of a \mathbb{Z}_2 topological invariant

$$\nu = \text{sgn} \{ Pf[A(0)] Pf[A(\pi)] \}. \quad (12)$$

A change in ν coincides with a bulk gap closing at $k = 0$ or $k = \pi$, consistent with the analytical phase boundaries obtained from the bulk dispersion. From the explicit expressions for $Pf[A(0)]$ and $Pf[A(\pi)]$, we can find that the nontrivial phase ($\nu = -1$) and trivial phase ($\nu = 1$) are separated by the critical lines

$$\begin{cases} \mu^2 = 4t^2 + (\gamma_1 - \gamma_2)^2, \\ \mu^2 = -4\Delta^2 + (\gamma_1 + \gamma_2)^2, \end{cases} \quad (13)$$

which are consistent with the gap closing points obtained from the energy spectrum in momentum space. The two critical lines intersect only when the condition $t^2 + \Delta^2 = \gamma_1\gamma_2$ is satisfied. Consequently, for $\gamma_1\gamma_2 \leq 0$, the two phase boundaries never cross, ensuring the persistence of a finite topologically nontrivial region in parameter space.

Figure 7 presents the phase diagrams in the $\mu - \gamma_1$ plane for $\gamma_2 = 0$ and $\gamma_2 = 1$. From the phase diagram, we can see that as long as $\gamma_1\gamma_2 \leq 0$ —namely, when one pairing imbalance vanishes or the two imbalances have opposite signs—the topologically nontrivial phase always

ant, which can be formulated in terms of the Pfaffian of the antisymmetric matrix at the high-symmetric momenta $k = 0$ and π . The resulting invariant correctly captures the emergence of Majorana zero modes at the boundaries and reproduces the analytically determined phase boundaries. Therefore, despite its non-Hermitian nature, the model retains the features analogous to that of the Hermitian Kitaev chain, while exhibiting enriched spectral and boundary phenomena due to pairing imbalance.

In the present model, the BdG Hamiltonian can be cast into a skew-symmetric form, allowing the Pfaffian to be evaluated at high-symmetry momenta. Specifically, at the $k = 0, \pi$, the Hamiltonian obeys $h(k) = -\tau_x h^T(k) \tau_x$, which allows it to be brought into an antisymmetric form. Here τ_x is the Pauli matrix. Defining $A(k) = ih(k)\tau_x$, one finds that $A(k)$ satisfies $A(k) = -A^T(k)$ for $k = 0, \pi$, independent of whether $h(k)$ is Hermitian. Substituting $h(k)$ in Eq. 5 into $A(k)$, we have

$$A(k) = i \begin{bmatrix} 0 & -\mu & -t(1 + e^{-ik}) \\ -t(1 + e^{ik}) & 0 & -\mu \\ 0 & -t(1 + e^{-ik}) & (\Delta - \gamma_1) - (\Delta - \gamma_2)e^{-ik} \end{bmatrix} \quad (11)$$

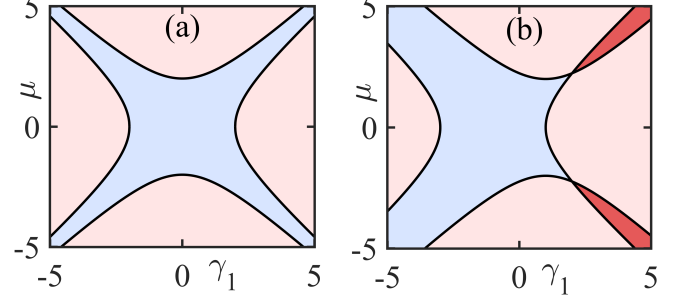


FIG. 7. (Color online) Topological phase diagram of the non-Hermitian Kitaev chain in the $\mu - \gamma_1$ plane for (a) $\gamma_2 = 0$ and (b) $\gamma_2 = 1$. The blue (pink) regions denote the topologically nontrivial (trivial) superconducting phase as determined by the Pfaffian Z_2 invariant. The red region in (b) is also trivial as the band is separated by imaginary line gap and there is no MZMs in the system. Other parameters are $t = 1$ and $\Delta = 1$.

survives, regardless of the strength of the chemical potential or pairing imbalance. The interplay between chemical potential and staggered pairing imbalance therefore stabilizes robust Majorana zero modes in a broad parameter regime. We note that in the red region of Fig. 7(b), the system is topologically trivial despite yielding $\nu = -1$ from the Pfaffian evaluation. In this parameter regime, $|\mu| < \sqrt{-4\Delta^2 + (\gamma_1 + \gamma_2)^2}$, the real part of the spectrum is gapless while the imaginary part remains gapped, and no MZMs appear under open boundary conditions.

V. SUMMARY

In summary, we have studied a one-dimensional non-Hermitian Kitaev chain with staggered imbalances in the p -wave superconducting pairing, which effectively introduce gain and loss into the pairing processes. By tuning the chemical potential and the pairing imbalance, we demonstrated that the system exhibits rich non-Hermitian spectral features, including real-complex transitions and the conversion between real and imaginary line gaps. The gap-closing points and transition boundaries were analytically determined from the momentum-space spectrum, and the numerical results under open boundary conditions were shown to be consistent with the bulk analysis. We further revealed that the introduction of pairing imbalance can significantly enhance the topological superconducting phase compared with the Hermitian Kitaev chain. In particular, the parameter region supporting Majorana zero modes is enlarged, and, remarkably, topologically nontrivial phases can persist even for arbitrarily large chemical potential when the pairing imbalance is staggered appropriately. This behavior is in sharp contrast to the Hermitian case, where the topological phase is restricted to a finite chemical-potential window. The topological phase boundaries were characterized by a \mathbb{Z}_2 invariant defined via the Pfaffian of the Bogoliubov-de Gennes Hamiltonian, yielding phase diagrams that are consistent with the bulk gap-closing conditions. In addition to Majorana zero modes, we also identified the coexistence of zero-energy and nonzero-energy Majorana edge modes in certain parameter regimes. These finite-energy edge states emerge as a direct consequence of the staggered non-Hermitian pairing and can persist even inside the bulk spectrum. By expressing the model in terms of Majorana fermion operators, we provided an intuitive picture for the origin

of these edge modes in terms of effective couplings in a Majorana ladder representation.

Experimentally, the staggered superconducting pairing considered in our model can be realized by proximitizing a one-dimensional semiconductor with a periodic array of superconductors, as proposed in Refs. [67, 68]. The spatially periodic deposition of superconducting islands naturally induces a staggered modulation of the pairing amplitude along the wire. Alternatively, the model may be implemented in quantum-dot-based platforms, where Majorana-like states have been observed in few-dot systems [87–90]. In such setups, effective pairing imbalance and dissipation can be engineered, allowing access to both zero-energy and finite-energy edge modes predicted here. The coexistence of these edge modes provides a setting to study non-Hermitian effects in topological superconductors and their influence on spectral and transport properties.

Our results demonstrate that non-Hermitian pairing imbalance can play a constructive role in stabilizing and enhancing topological superconducting phases, rather than merely destroying them. This work uncovers novel non-Hermitian topological phenomena in superconducting systems and provides a new platform for exploring Majorana physics and topological superconductivity beyond the Hermitian paradigm.

ACKNOWLEDGMENTS

This work is supported by the National Natural Science Foundation of China under Grant No. 12204326. R.L. is supported by the Quantum Science and Technology-National Science and Technology Major Project (Grant No. 2021ZD0302100) and the 'Gravitational Wave Detection' program (2023YFC2205800) funded by the Ministry of Science and Technology of the People's Republic of China.

[1] J. Alicea, New directions in the pursuit of Majorana fermions in solid state systems, *Rep. Prog. Phys.* **75**, 076501 (2012).

[2] C. W. J. Beenakker, Search for Majorana Fermions in Superconductors, *Annu. Rev. Condens. Matter Phys.* **4**, 113 (2013).

[3] S. R. Elliott and M. Franz, Colloquium: Majorana fermions in nuclear, particle, and solid-state physics, *Rev. Mod. Phys.* **87**, 137 (2015).

[4] Y. Ando and L. Fu, Topological Crystalline Insulators and Topological Superconductors: From Concepts to Materials, *Annu. Rev. Condens. Matter Phys.* **6**, 361 (2015).

[5] M. Sato and Y. Ando, Topological superconductors: a review, *Rep. Prog. Phys.* **80**, 076501 (2017).

[6] A. Yazdani, F. von Oppen, B. I. Halperin, and A. Yacoby, Hunting for Majorana fermions, *Science* **380**, 6651 (2023).

[7] J. Alicea, Y. Oreg, G. Refael, F. Von Oppen, and M. Fisher, Non-Abelian statistics and topological quantum information processing in 1D wire networks, *Nat. Phys.* **7**, 412 (2011).

[8] S. Das Sarma, M. Freedman, and C. Nayak, Majorana zero modes and topological quantum computation, *npj Quantum Inf.* **1**, 15001 (2015).

[9] T. E. O'Brien, P. Rožek, and A. R. Akhmerov, Majorana-Based Fermionic Quantum Computation, *Phys. Rev. Lett.* **120**, 220504 (2018).

[10] B. Lian, X.-Q. Sun, A. Vaezi, X.-L. Qi, and S.-C. Zhang, Topological quantum computation based on chiral Majorana fermions, *Proc. Natl. Acad. Sci. U.S.A.* **115**, 10938 (2018).

[11] D. Litinski and F. von Oppen, Quantum computing with Majorana fermion codes, *Phys. Rev. B* **97**, 205404 (2018).

[12] N. Read and D. Green, Paired states of fermions in two dimensions with breaking of parity and time-reversal

symmetries and the fractional quantum Hall effect, *Phys. Rev. B* **61**, 10267 (2000).

[13] M. Stone and R. Roy, Edge modes, edge currents, and gauge invariance in $p_x + ip_y$ superfluids and superconductors, *Phys. Rev. B* **69**, 184511 (2004).

[14] P. Fendley, M. P. A. Fisher, and C. Nayak, Edge states and tunneling of non-Abelian quasiparticles in the $\nu = 5/2$ quantum Hall state and $p+ip$ superconductors, *Phys. Rev. B* **75**, 045317 (2007).

[15] L. Fu and C. L. Kane, Superconducting proximity effect and Majorana fermions at the surface of a topological insulator, *Phys. Rev. Lett.* **100**, 096407 (2008).

[16] J. D. Sau, R. M. Lutchyn, S. Tewari, and S. Das Sarma, Generic new platform for topological quantum computation using semiconductor heterostructures, *Phys. Rev. Lett.* **104**, 040502 (2010).

[17] J. D. Sau, S. Tewari, R. M. Lutchyn, T. D. Stanescu, and S. Das Sarma, Non-Abelian quantum order in spin-orbit-coupled semiconductors: Search for topological Majorana particles in solid-state systems, *Phys. Rev. B* **82**, 214509 (2010).

[18] R. M. Lutchyn, J. D. Sau, and S. Das Sarma, Majorana fermions and a topological phase transition in semiconductor-superconductor heterostructures *Phys. Rev. Lett.* **105**, 077001 (2010).

[19] Y. Oreg, G. Refael, and F. von Oppen, Helical liquids and Majorana bound states in quantum wires, *Phys. Rev. Lett.* **105**, 177002 (2010).

[20] S. B. Chung, H. J. Zhang, X. L. Qi, and S. C. Zhang, Topological superconducting phase and Majorana fermions in half-metal/superconductor heterostructures, *Phys. Rev. B* **84**, 060510(R) (2011).

[21] S. Raghu, A. Kapitulnik, and S. A. Kivelson, Hidden Quasi-One-Dimensional Superconductivity in Sr_2RuO_4 , *Phys. Rev. Lett.* **105**, 136401 (2010).

[22] N. B. Kopnin and M. M. Salomaa, Mutual friction in superfluid 3He : Effects of bound states in the vortex core, *Phys. Rev. B* **44**, 9667 (1991).

[23] X. L. Qi, T. L. Hughes, S. Raghu, and S. C. Zhang, Time-reversal-invariant topological superconductors and superfluids in two and three dimensions, *Phys. Rev. Lett.* **102**, 187001 (2009).

[24] S. B. Chung and S. C. Zhang, Detecting the Majorana fermion surface state of 3He through spin relaxation, *Phys. Rev. Lett.* **103**, 235301 (2009).

[25] C. W. Zhang, S. Tewari, R. M. Lutchyn, and S. Das Sarma, $p_x + ip_y$ superfluid from s -wave interactions of fermionic cold atoms, *Phys. Rev. Lett.* **101**, 160401 (2008).

[26] M. Sato, Y. Takahashi, and S. Fujimoto, Non-Abelian topological order in s -wave superfluids of ultracold fermionic atoms, *Phys. Rev. Lett.* **103**, 020401 (2009).

[27] X. J. Liu, L. Jiang, H. Pu, and H. Hu, Probing Majorana fermions in spin-orbit-coupled atomic Fermi gases, *Phys. Rev. A* **85**, 021603(R) (2012).

[28] C. Qu, Z. Zheng, M. Gong, Y. Xu, L. Mao, X. Zou, G. Guo, and C. Zhang, Topological superfluids with finite-momentum pairing and Majorana fermions, *Nat. Commun.* **4**, 2710 (2013).

[29] C. Chen, Inhomogeneous topological superfluidity in one-dimensional spin-orbit-coupled Fermi gases, *Phys. Rev. Lett.* **111**, 235302 (2013).

[30] C. Qu, M. Gong, Y. Xu, S. Tewari, and C. W. Zhang, Majorana fermions in quasi-one-dimensional and higher-dimensional ultracold optical lattices, *Phys. Rev. A* **92**, 023621 (2015).

[31] J. Ruhman, E. Berg, and E. Altman, Topological states in a one-dimensional Fermi gas with attractive interaction, *Phys. Rev. Lett.* **114**, 100401 (2015).

[32] S. Nadj-Perge, I. K. Drozdov, B. A. Bernevig, and A. Yazdani, Proposal for realizing Majorana fermions in chains of magnetic atoms on a superconductor, *Phys. Rev. B* **88**, 020407(R) (2013).

[33] H. Y. Hui, P. M. R. Brydon, J. D. Sau, S. Tewari, and S. Das Sarma, Majorana fermions in ferromagnetic chains on the surface of bulk spin-orbit coupled s -wave superconductors, *Sci. Rep.* **5**, 8880 (2015).

[34] E. Dumitrescu, B. Roberts, S. Tewari, J. D. Sau, and S. Das Sarma, Majorana fermions in chiral topological ferromagnetic nanowires, *Phys. Rev. B* **91**, 094505 (2015).

[35] P. A. Ioselevich and M. V. Feigel'man, Anomalous Josephson current via Majorana bound states in topological insulators, *Phys. Rev. Lett.* **106**, 077003 (2011).

[36] A. Zazunov, A. L. Yeyati, and R. Egger, Coulomb blockade of Majorana-fermion-induced transport, *Phys. Rev. B* **84**, 165440 (2011).

[37] B. H. Wu and J. C. Cao, Tunneling transport through superconducting wires with Majorana bound states, *Phys. Rev. B* **85**, 085415 (2012).

[38] Pablo San-Jose, Elsa Prada, and Ramón Aguado, ac Josephson effect in finite-length nanowire junctions with Majorana modes, *Phys. Rev. Lett.* **108**, 257001 (2012).

[39] A. Ueda and T. Yokoyama, Anomalous interference in Aharonov-Bohm rings with two Majorana bound states, *Phys. Rev. B* **90**, 081405(R) (2014).

[40] Q.-B. Zeng, S. Chen, L. You, and R. Lü, Transport through a quantum dot coupled to two Majorana bound states, *Front. Phys.* **12**, 127302 (2016).

[41] V. Mourik, K. Zuo, S. M. Frolov, S. R. Plissard, E. P. A. M. Bakkers, and L. P. Kouwenhoven, Signatures of Majorana fermions in hybrid superconductor-semiconductor nanowire devices, *Science* **336**, 1003 (2012).

[42] M. T. Deng, C. L. Yu, G. Y. Huang, M. Larsson, P. Caroff, and H. Q. Xu, Anomalous zero-bias conductance peak in a Nb -InSb nanowire-Nb hybrid device, *Nano Lett.* **12**, 6414 (2012).

[43] L. P. Rokhinson, X. Liu, and J. K. Furdyna, The fractional ac Josephson effect in a semiconductor-superconductor nanowire as a signature of Majorana particles, *Nat. Phys.* **8**, 795 (2012).

[44] A. Das, Y. Ronen, Y. Most, Y. Oreg, M. Heiblum, and H. Shtrikman, Zero-bias peaks and splitting in an Al-InAs nanowire topological superconductor as a signature of Majorana fermions, *Nat. Phys.* **8**, 887 (2012).

[45] A. D. K. Finck, D. J. Van Harlingen, P. K. Mohseni, K. Jung, and X. Li, Anomalous modulation of a zero-bias peak in a hybrid nanowire-superconductor device, *Phys. Rev. Lett.* **110**, 126406 (2013).

[46] S. Nadj-Perge, I. K. Drozdov, J. Li, H. Chen, S. Jeon, J. Seo, A. H. MacDonald, B. A. Bernevig, and A. Yazdani, Observation of Majorana fermions in ferromagnetic atomic chains on a superconductor, *Science* **346**, 602 (2014).

[47] Z. Cao, S. Chen, G. Zhang, and D. E. Liu, Recent progress on Majorana in semiconductor-superconductor heterostructures—engineering and detection, *Sci. China Phys. Mech. Astron.* **66**, 267003 (2023).

[48] L. Kouwenhoven, Perspective on Majorana bound-states

in hybrid superconductor-semiconductor nanowires, *Mod. Phys. Lett. B* **39**, 2540002 (2025).

[49] A. Y. Kitaev, Unpaired Majorana fermions in quantum wires, *Phys. Usp.* **44**, 131 (2001).

[50] A. R. Akhmerov, J. P. Dahlhaus, F. Hassler, M. Wimmer, and C. W. J. Beenakker, Quantized conductance at the Majorana phase transition in a disordered superconducting wire, *Phys. Rev. Lett.* **106**, 057001 (2011).

[51] X. Cai, L.-J. Lang, S. Chen, and Y. Wang, Topological superconductor to Anderson localization transition in one-dimensional incommensurate lattices, *Phys. Rev. Lett.* **110**, 176403 (2013).

[52] W. DeGottardi, D. Sen, and S. Vishveshwara, Majorana fermions in superconducting 1D systems having periodic, quasiperiodic, and disordered potentials, *Phys. Rev. Lett.* **110**, 146404 (2013).

[53] J. Wang, X.-J. Liu, G. Xianlong, and H. Hu, Phase diagram of a non-Abelian Aubry-André-Harper model with p-wave superfluidity, *Phys. Rev. B* **93**, 104504 (2016).

[54] Q.-B. Zeng, S. Chen, and R. Lü, Generalized Aubry-André-Harper model with p-wave superconducting pairing, *Phys. Rev. B* **94**, 125408 (2016).

[55] Q.-B. Zeng, R. Lü, and L. You, Topological superconductors in one-dimensional mosaic lattices, *Europhysics Letters* **135**, 17003 (2021).

[56] D. Vodola, L. Lepori, E. Ercolessi, A. V. Gorshkov, and G. Pupillo, Kitaev chains with long-range pairing, *Phys. Rev. Lett.* **113**, 156402 (2014).

[57] A. Alecce and L. Dell'Anna, Extended Kitaev chain with longer-range hopping and pairing, *Phys. Rev. B* **95**, 195160 (2017).

[58] A. Dutta and A. Dutta, Probing the role of long-range interactions in the dynamics of a long-range Kitaev chain, *Phys. Rev. B* **96**, 125113 (2017).

[59] J. Fraxanet, U. Bhattacharya, T. Grass, M. Lewenstein, and A. Dauphin, Localization and multifractal properties of the long-range Kitaev chain in the presence of an Aubry-André-Harper modulation, *Phys. Rev. B* **106**, 024204 (2022).

[60] G. Francica and L. Dell'Anna, Correlations, long-range entanglement, and dynamics in long-range Kitaev chains, *Phys. Rev. B* **106**, 155126 (2022).

[61] Y.-H. Huang, Y.-T. Zou, and C. Ding, Dynamical relaxation of a long-range Kitaev chain, *Phys. Rev. B* **109**, 094309 (2024).

[62] D.-P. Liu, Topological phase boundary in a generalized Kitaev model, *Chinese Phys. B* **25**, 057101 (2016).

[63] B.-Z. Zhou and B. Zhou, Topological phase transition in a ladder of the dimerized Kitaev superconductor chains, *Chinese Phys. B* **25**, 107401 (2016).

[64] B.-Z. Zhou, D.-H. Xu, and B. Zhou, Majorana zero modes in a ladder of density-modulated Kitaev superconductor chains, *Phys. Lett. A* **381**, 2426 (2017).

[65] O. Lesser and Y. Oreg, Universal phase diagram of topological superconductors subjected to magnetic flux, *Phys. Rev. Research* **2**, 023063 (2020).

[66] S. Hoffman, J. Klinovaja, and D. Loss, Topological phases of inhomogeneous superconductivity, *Phys. Rev. B* **93**, 165418 (2016).

[67] Y. Levine, A. Haim, and Y. Oreg, Realizing topological superconductivity with superlattices, *Phys. Rev. B* **96**, 165147 (2017).

[68] S. D. Escribano, A. Levy Yeyati, Y. Oreg, and E. Prada, Effects of the electrostatic environment on superlattice Majorana nanowires, *Phys. Rev. B* **100**, 045301 (2019).

[69] X.-J. Zhang, R. Lü, and Q.-B. Zeng, Majorana edge modes in one-dimensional Kitaev chain with staggered p-wave superconducting pairing, *J. Phys.: Condens. Matter* **37**, 425501 (2025).

[70] H. Cao and J. Wiersig, Dielectric microcavities: Model systems for wave chaos and non-Hermitian physics, *Rev. Mod. Phys.* **87**, 61 (2015).

[71] V. V. Konotop, J. Yang, and D. A. Zezyulin, Nonlinear waves in PT-symmetric systems, *Rev. Mod. Phys.* **88**, 035002 (2016).

[72] Y. Ashida, Z. Gong, and M. Ueda, Non-Hermitian physics, *Adv. Phys.* **69**, 249 (2020).

[73] E. J. Bergholtz, J. C. Budich, and F. K. Kunst, Exceptional topology of non-Hermitian systems, *Rev. Mod. Phys.* **93**, 015005 (2021).

[74] W. D. Heiss, The physics of exceptional points, *J. Phys. A: Math. Theor.* **45**, 444016 (2012).

[75] S. Yao and Z. Wang, Edge states and topological invariants of non-Hermitian systems, *Phys. Rev. Lett.* **121**, 086803 (2018).

[76] S. Yao, F. Song, and Z. Wang, Non-Hermitian Chern bands, *Phys. Rev. Lett.* **121**, 136802 (2018).

[77] K. Kawabata, K. Shiozaki, M. Ueda, M. Sato, Symmetry and topology in non-Hermitian physics, *Phys. Rev. X* **9**, 041015 (2019).

[78] X. Wang, T. Liu, Y. Xiong, and P. Tong, Spontaneous PT-symmetry breaking in non-Hermitian Kitaev and extended Kitaev models, *Phys. Rev. A* **92**, 012116 (2015).

[79] Q.-B. Zeng, B. Zhu, S. Chen, L. You, and R. Lü, Non-Hermitian Kitaev chain with complex on-site potentials, *Phys. Rev. A* **94**, 022119 (2016).

[80] C. Li, X. Z. Zhang, G. Zhang, and Z. Song, Topological phases in a Kitaev chain with imbalanced pairing, *Phys. Rev. B* **97**, 115436 (2018).

[81] N. Shibata and H. Katsura, Dissipative spin chain as a non-Hermitian Kitaev ladder, *Phys. Rev. B* **99**, 174303 (2019).

[82] X.-M. Zhao, C.-X. Guo, S.-P. Kou, L. Zhuang, and W.-M. Liu, Defective Majorana zero modes in a non-Hermitian Kitaev chain, *Phys. Rev. B* **104**, 205131 (2021).

[83] Y. B. Shi and Z. Song, Fixed lines in a non-Hermitian Kitaev chain with spatially balanced pairing processes, *Phys. Rev. B* **108**, 125121 (2023).

[84] Y. B. Shi and Z. Song, Topological phase in a Kitaev chain with spatially separated pairing processes, *Phys. Rev. B* **107**, 125110 (2023).

[85] S. Sayyad and J. L. Lado, Topological phase diagrams of exactly solvable non-Hermitian interacting Kitaev chains, *Phys. Rev. Research* **5**, L022046 (2023).

[86] J. Cayao and R. Aguado, Non-Hermitian minimal Kitaev chains, *arXiv: 2406.18974* (2024).

[87] T. Dvir et al., Realization of a minimal Kitaev chain in coupled quantum dots, *Nature* **614**, 445 (2023).

[88] S. L. D. T. Haaf et al., A two-site Kitaev chain in a two-dimensional electron gas, *Nature* **630**, 329 (2024).

[89] F. Zatelli et al., Robust poor man's Majorana zero modes using Yu-Shiba-Rusinov states, *Nat. Com.* **15**, 7933 (2024).

[90] A. Bordin et al., Enhanced Majorana stability in a three-site Kitaev chain, *Nat. Nanotech.* (2025).